IN ORBIT TESTING OF SOLID DEBRIS DETECTOR

Waldemar Bauer [a)], Vitali Braun [b)], Philipp Werner [c)], Sergio Montenegro [d)], Merlin F. Barschke [c,e)], Oliver Romberg [a)], Erik Dilger [d)]

a) German Aerospace Center (DLR), Institute of Space Systems, Robert-Hooke-Str. 7, 28359 Bremen, Germany, waldemar.bauer@dlr.de, oliver.romberg@dlr.de

b) IMS Space Consultancy GmbH at ESA Space Debris Office, Robert-Bosch-Str. 5, 64293 Darmstadt, Germany vitali.braun@esa.int

c) Technische Universität Berlin, Chair of Space Technology, Straße des 17. Juni 135, 10623 Berlin, Germany, philipp.werner@tu-berlin.de, merlin.barschke@tu-berlin.de

d) Universität Wuerzburg, Aerospace Information Technology, Würzburg, Germany, sergio.montenegro@uni-wuerzburg.de, erik.dilger@uni-wuerzburg.de

e) Deutsches Elektronen-Synchrotron DESY, Platanenallee 6, 15738 Zeuthen, Germany, merlin.barschke@desy.de

The number of artificial objects in space increases due to past and present space activities. To analyse the quantity of the small (diameter > 100µm up to cm) space debris and meteoroids, an innovative in-situ impact detection method has been developed at DLR (German Aerospace Center) in Bremen, Germany. The method Solar panel-based Impact Detector "SOLID" uses solar panels for impact detection. Since solar panels provide large detection areas and exist on nearly all satellites, this method enables for the collection of large amounts of data in different orbits. An impacting object generates a permanent damage on a panel. The damage can be determined during analysis scan as well as confirmed or refuted in the frame of subsequent scans of the panels. Those properties of the sensor system can significantly improve the amount as well as the quality of measurement data to be used for environmental model validation. The SOLID method was successfully verified on ground by Hypervelocity Impact (HVI) tests at Fraunhofer EMI, Freiburg, Germany. The ability of the detection method SOLID for impact detection of space debris and meteoroids was clearly demonstrated on ground. Since July 2017, the SOLID sensor system is placed in a 600 km Sun-synchronous orbit on the microsatellite mission TechnoSat of Technische Universität Berlin (TUB). Four solar panels equipped with SOLID technology are installed on the satellite for in-orbit testing and environmental exploration. The total detection area of all panels is about 0.0755m². The system was designed to detect space debris or meteoroid objects with a diameter larger than 100 µm. In total 15,570,047 scans were performed over the four years in space. By means of measurement data changes were identified on one panel. However, so far, the telemetry data shows no clear evidence for an impact.

Keywords: SOLID, space debris, in-situ impact detector, solar panels, hypervelocity impact, satellite subsystems

I. INTRODUCTION

The small object population of the Meteoroid And Space Debris Terrestrial Environment Reference Model (MASTER) is currently solely validated by crater and holes counts from several returned surfaces [1, 2]. While there have been measurements by in-situ detectors like Debris In-orbit Evaluator (DEBIE) [3–5] or Geostationary Orbit Impact Detector (GORID) [6], none of them found their way yet into the MASTER validation process . This is currently under preparation for the next upgrade of the MASTER model [1, 2, 7] in the frame of the Debris Mitigation Facility (DMF), under the ESA activity DMF-04, and will include in-situ measurements from in-situ sensors.

From Low Earth Orbit (LEO) returned and inspected surfaces are solar panels of the Hubble Space Telescope (HST) and EuReCa (European Retrievable Carrier), as well as different surface panels from LDEF (Long Duration Exposure Facility). LDEF was in orbit between 1984 and 1990 and provided a rich data based on many surfaces and dedicated experiments that have been inspected for craters and holes. The latter include the Interplanetary Dust Experiment (IDE), which also correlated impacts with timestamps and latter allowed to associate clusters of impacts with individual SRM

firings [8]. The HST was launched in 1990 and experienced several service missions (SM) by the Space Shuttle during its operational lifetime. During the famous SM1 in December 1993, a corrective optics was installed for Hubble. At the same time, the solar panels contributed to the mission by ESA, were replaced. One of the solar panels was recovered for inspection while the second burned up in the atmosphere. During the SM3B service mission in 2002, the solar panels were replaced again, this time after spending about 8 years in orbit. Both HST panels of the SM3B mission were recovered and became accessible for inspection. In a similar manner, ESA's EuReCa mission was launched in July 1992 and recovered one year later by the Space Shuttle. Table 1 shows a summary of retrieved hardware from space for inspection. Identified damages (crater, hole) caused by impacts of space debris or meteoroids were measured, classified and utilised for MASTER validation.

Table 1: Retrieved surfaces from space: D_M = duration in orbit, h =Altitude, i =inclination, A_{tot}= total exposed area [9–12]

Spacecraft	Mission			Orbit		Area
	Start	*Ende*	D_M (days)	h (km)	i (°)	$A_{tot}(m^2)$
LDEF	06.04.1984	12.01.1990	2106	475	28,5	151
HST (SM1)	24.04.1990	08.12.1993	1320	614	28,5	62
EuReCa	01.08.1992	24.06.1993	326	495	28,5	131
HST (SM3B)	04.12.1993	03.03.2002	3011	614	28,5	120

Table 2 shows a comparison of utilised validation data for ESAs MASTER and NASAs Orbital Debris Engineering Model (ORDEM).

Table 2: Utilized data for environmental models validation for objects $\leq 1\ mm$ [2, 13–15]

Small Objects Validation			
MASTER-8.0.2		ORDEM-3.1	
LDEF	LEO	STS windows / radiator	LEO
EuReCa	LEO	EuReCa qualitatively	LEO
HST-SA (SM1) HST-SA (SM3B)	LEO	HST-SA, MLI cover / radiator	LEO
		MEEP* qualitatively	LEO

* MEEP: Mir Experiments Exposure Package

In summary it can be stated that the currently available measurement data is insufficient. However, the collision probability with small objects (diameter > 100µm up to cm) is high and is even increasing with growing space exploitation. Furthermore, degradation or significant damage of spacecraft or payload can be expected in case of collision with objects > 100µm (for instance, optical lenses are more susceptible to impacts from smaller objects). Since the ground-based measurement capabilities in that size regime are limited, in-situ measurement sensors are required to provide data in the range 100µm up to 1 cm [9].

II. GROUND TESTING

To address this need and to close the existing data gap an innovative debris detector was developed and patented [16, 17] at DLR. The Solar panel-based Impact Detector (SOLID) is an in-situ sensor system. As shown in Figure 1, SOLID utilizes subsystems of a satellite [9, 18, 19] to measure space debris and meteoroids impacts in space.

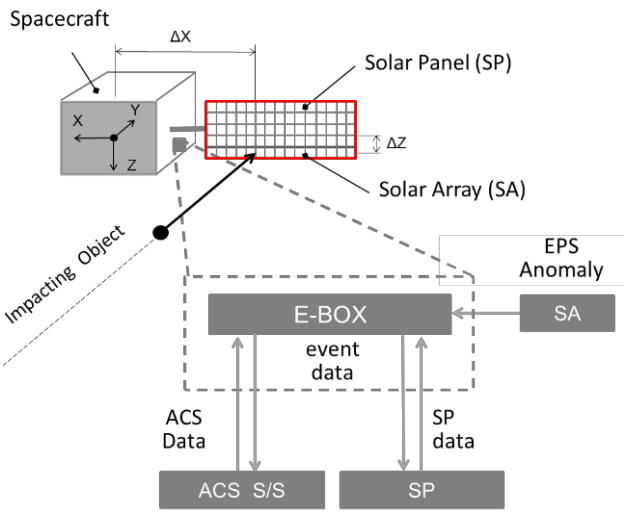

Figure 1: SOLID concept [9, 18, 20]

The core element of the SOLID system is a solar panel with integrated detection layers. Figure 2 shows schematically an EuReCa based solar panel design adapted for impact detection. An impacting debris or meteoroid object generates permanent damage on a solar panel. Depending on object diameter and density, impact velocity, and impact geometry a damage can vary from small cratering of the solar cell cover glass up to a clear hole penetration of the solar panel. In case of sufficiently large kinetic energy of an impactor the detection layers behind the solar cells will be permanently destroyed [21]. By identification of severed lines of the detection layer the damage size can be estimated. Subsequently an impactor diameter can be calculated by utilization of the ESA developed damage equations [10, 11]. The verification of the SOLID detection method was successfully performed by Hypervelocity Impact (HVI) tests in 2013 at Fraunhofer EMI, Freiburg, Germany

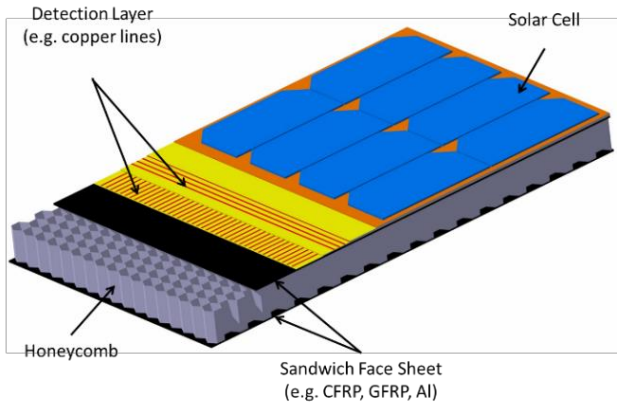

Figure 2: SOLID solar panel [9, 18]

. Figure 3 shows a clear hole on a SOLID prototype panel as an example. More detailed information can be found in [21].

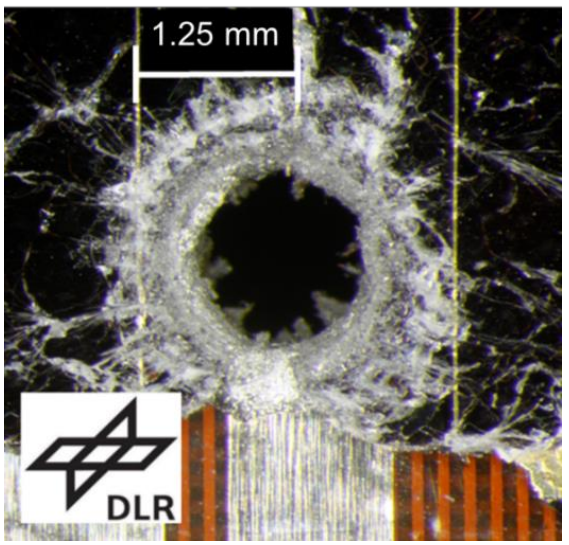

Figure 3: Clear hole damage on a test SOLID solar panel generated by a glass projectile: $\boldsymbol{d_p}$ ~ 500 µm, $\boldsymbol{v_p}$ ~ 4 km/s, $\boldsymbol{\varrho_p}$ = 2.5 g/cm³ [21]

III. IN ORBIT TESTING

The first In Orbit Testing (IOT) of the SOLID system has been performed on the microsatellite mission TechnoSat [22–25] of Technische Universität Berlin. The satellite was launched aboard a Russian Soyuz 2.1 rocket on Friday, July 14th 2017 at 8:36 am Central European Summer Time (CEST) into a 600 km Sun-synchronous orbit [26]. The launch mass of the satellite is 20 kg and its outer dimensions are 465 × 465 × 305 mm³ (without antennas). TechnoSat carries seven different payloads for IOT [22–25] and was designed for a mission duration of one year. However, after over four years in orbit the satellite is still performing well and continues to provide data from SOLID.

Figure 4 shows the final preparation of TechnoSat for launch (a), the stack of accommodated satellites on the upper stage without (b) and with (c) the fairing as well as the launch of the Soyuz rocket from Baikonur cosmodrome in Kazakhstan, with TechnoSat aboard (d).

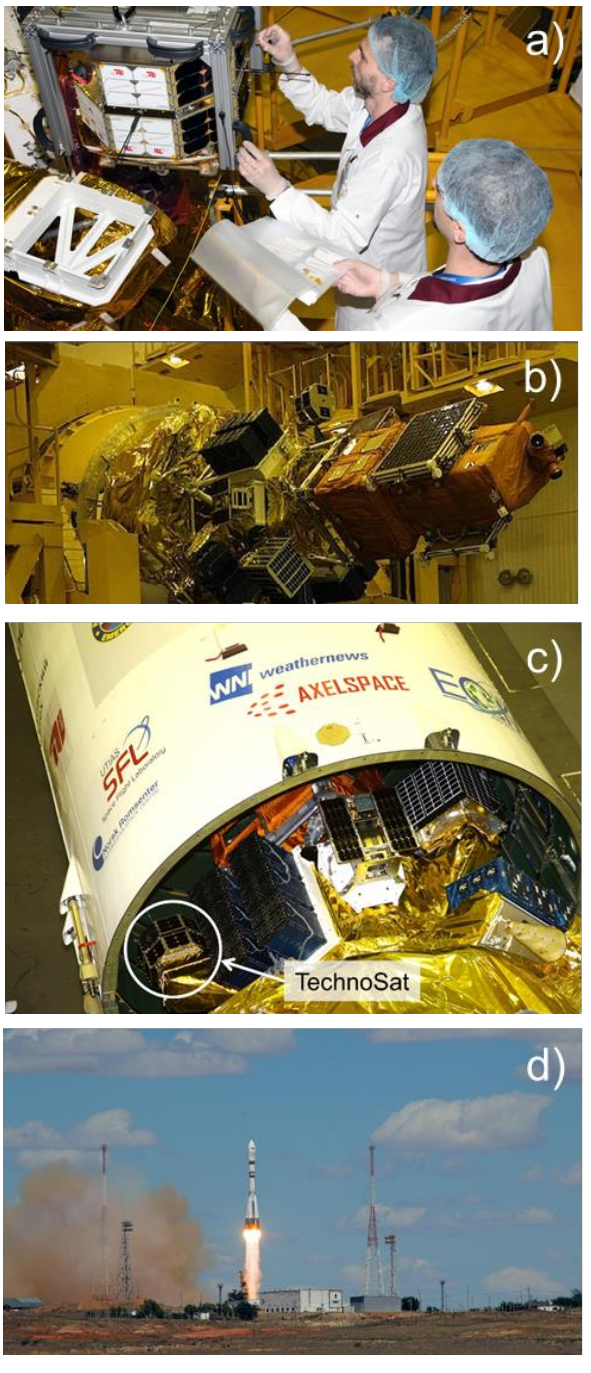

Figure 4: Launch preparation and launch of TechnoSat mission with SOLID aboard [27, 28] (Image credit: Roscosmos)

The satellite is equipped with 17 solar panels. Each of the 17 panels includes six solar cells, which are glued to the printed circuit board (PCB) substrate. The PCB again is glued to an aluminium sheet to increase mechanical stability of the panels. Four of the 17 solar panels are adapted for space debris and meteoroid impact detection by utilization of the SOLID technology. The detection layers of a panel are covered by six solar cells (162.5 mm x 126 mm). Figure 5 shows digital rendering of the satellite.

Figure 5: Digital rendering of the TechnoSat mission satellite of the Technische Universität Berlin [29]

Figure 6 shows the nadir pointing view of the satellite with four laterally accommodated SOLID detection panels (top) as well as a panel (bottom left) with an enlarged section view showing the X and Y detection lines behind the solar cells (bottom right).

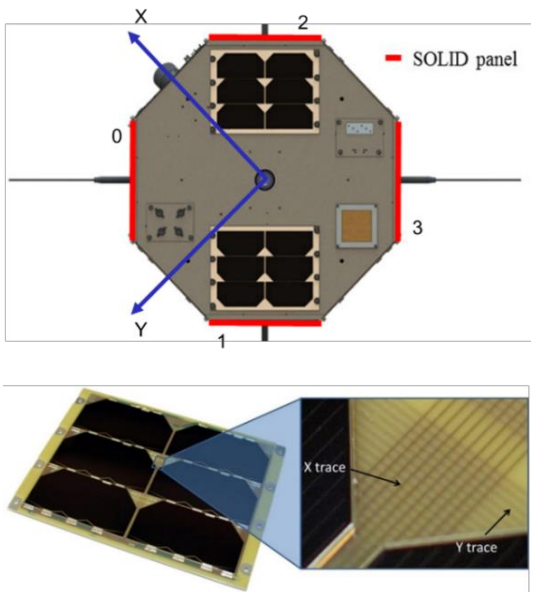

Figure 6: Accommodated solar panels with SOLID technology on the TechnoSat (top), manufactured panel (bottom left) and enlarged section view of the detection layers (bottom right) [30]

The electronic components and plugs are accommodated on the back side of the solar panels within the cut-out of the aluminium sheet as shown in Figure 7.

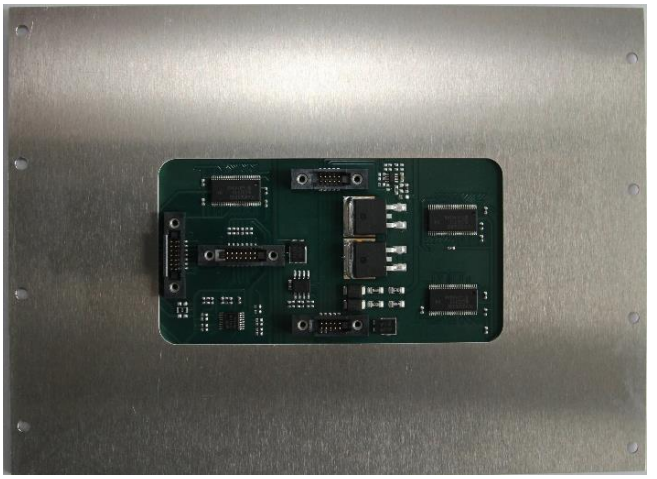

Figure 7: Back side of a TechnoSat solar panel with SOLID technology

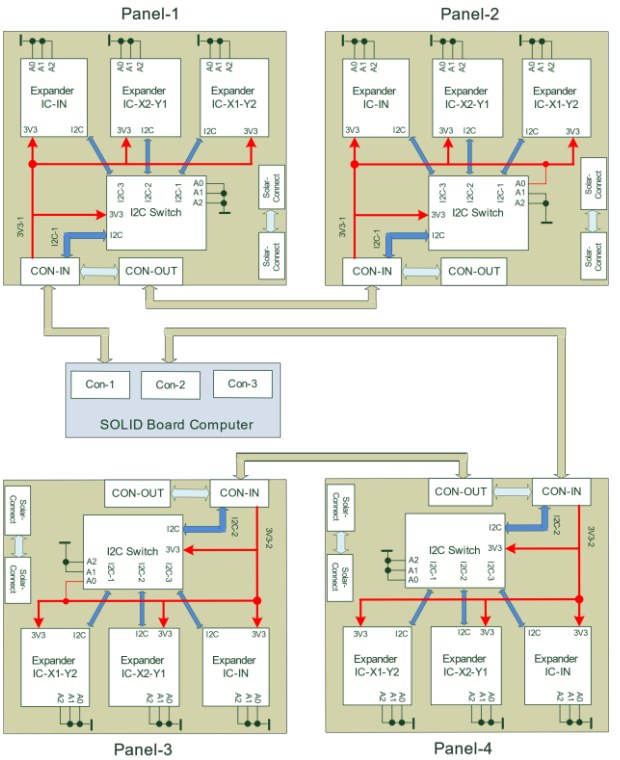

Figure 8: Schematic view of the detection panels [30]

The four detection panels (0, 1, 2 and 3) are connected to and controlled by a dedicated computational node with two cold redundant microcontrollers. The hardware of the SOLID node is identical to the On-Board Computer (OBC) of

TechnoSat and thereby easily integrated into the overall satellite bus design. The detection panels are connected to two I2C busses in pairs. The panels are analysed one after another and the data is stored on OBC for subsequent downlink.

Figure 9 shows schematically the structure of the detection lines on one panel as implemented for the TechnoSat mission. The width of the lines in X and Y directions is 100 µm. The distance of the lines is 500 µm and 350 µm respectively. In total, there are ten groups for each axis, whereby X and Y axis are subdivided additionally into X 1, X 2 and Y1, Y 2 respectively. Using output expanders, the voltage is applied to the nodes (red dot in Figure 9) and can be analysed with input expanders within each group (X 1-..; Y 2-..; X 2-..; Y 1-..). In this way, each individual line can be analysed, if the detection line is severed because of an impact or if it is still intact.

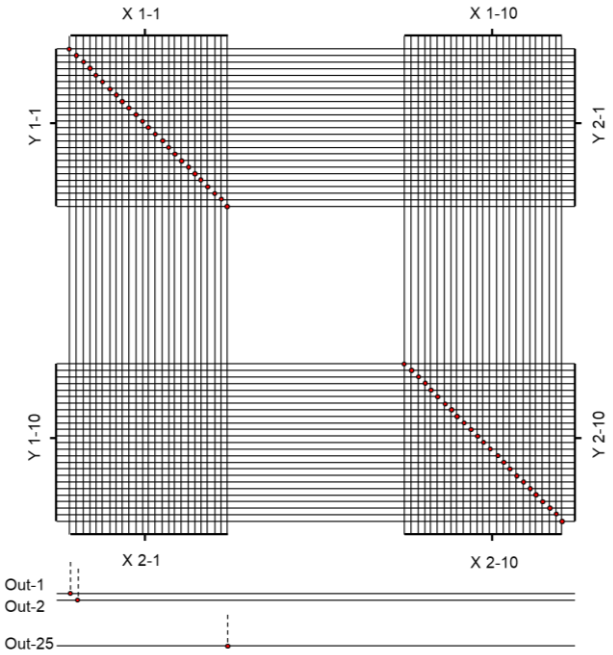

Figure 9: Schematic view of detection lines structure

Figure 10 shows the SOLID software architecture. The generated data can be subdivided into the standard telemetry (STM) and the extended telemetry (ETM). The STM is generated in regular intervals and contains basic overview information of the SOLID application, like scan-counter, error-counter and total severed lines counter. The ETM is generated on telecommand (TC) request (real time telemetry) or in case a change of detection line state was identified (history telemetry).

The SOLID software was implemented in the satellite's software network of Building Blocks (BB) applications. Several of such applications belong to the common software configuration of all computational nodes within the satellite bus, implementing tasks common to all nodes. All applications communicate with other applications independent of their location on the same or another node via the publisher subscriber protocol of the Realtime Onboard Dependable Operating System's (RODOS) middleware [31].

The utilized SOLID software performs sequential scans of the detection lines in each panel using predefined settings. The verification of the detection line state occurs by using input and output expanders and applying voltage to each individual line (see also Figure 8 and Figure 9). In this way two states of the lines can be identified by the SOLID system: Intact or severed (cut through) line. Once a state change compared to the previous state is identified, a report is automatically generated (history telemetry) for the corresponding panel. Furthermore, every 12 hours a report for each panel is produced independently of detection lines state (history telemetry). The state of each panel is also saved in non-volatile memory and reloaded on each restart of the SOLID node. Each report includes among others the following information as result of the latest scan of a panel:

- the state of each individual detection line (intact or severed),
- the total number of detection lines changes per scan compared to the previous scan state,
- the timestamp of the identified latest change named "Last change",
- the incremental count of scans since activation of the SOLID node,
- the timestamp of the send telemetry named "TM Time".

The automatically generated reports are saved on satellite's On-Board Computer (OBC) as history data until the data is transmitted to a ground station. Additionally, the latest available report for each individual panel can be requested by an operator via telecommand during a pass over a ground station as real time data. The reports are then directly downlinked without storage in the OBC.

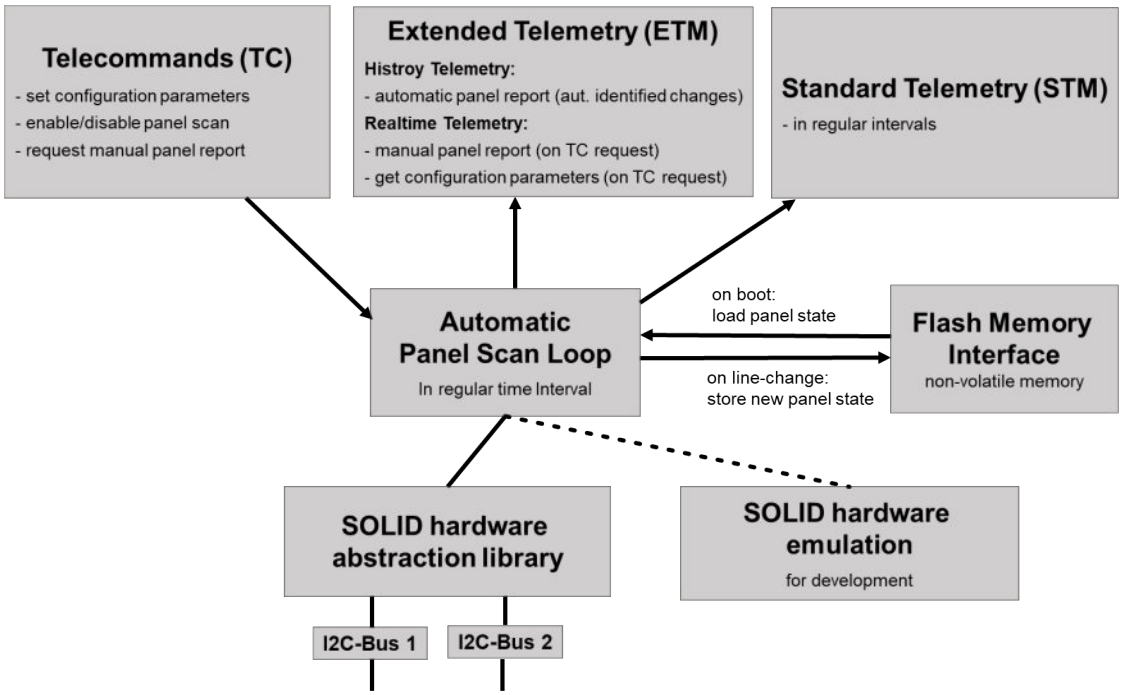

Figure 10: SOLID software architecture

IV. MEASUREMENT RESULTS

The commissioning of the microsatellite bus of the TechnoSat mission was started on July 14th 2017. Subsequently the 7 payloads were switched on step by step and performed their commissioning procedures. The SOLID node was first enabled on August 10th, 2017 at 07:56:00 UTC and the experiment performed 30 seconds later for the first time the in-orbit measurements.

As of July 2021, there is almost four years (10.08.2017-08.07.2021) of in orbit measurement data available. Table 3 summarizes the total number of logged scans during this time.

Table 3: Annual number of logged scans by end of the years: 2017, 2018, 2019, 2020 and 2021

Number of Scans		
Year	Per year	Accumulated
2017	1,236,650	1,236,650
2018	4,554,173	5,790,823
2019	3,136,881	8,927,704
2020	4,866,325	13,794,029
2021*	1,776,018	15,570,047

*Until 08.07.2021

Since start in 2017, the SOLID system has been operated almost continuously throughout the four years in orbit. There are only few shorter and one longer time periods of no operation as shown in Figure 11.

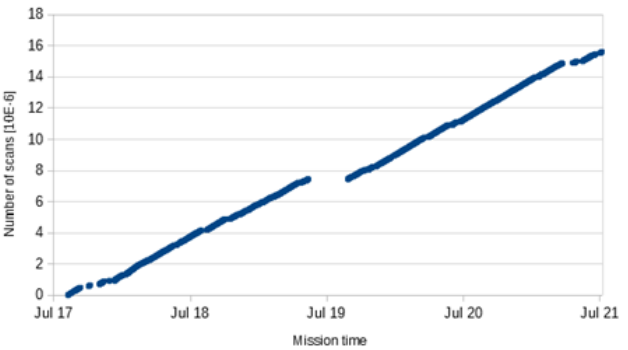

Figure 11: Commutative number of performed SOLID scans in time period 08.2017-07.2021

Initially the SOLID node and the panels scans were set up and enabled by an operator manually during a ground station pass. However, in case of any contingency detected by the satellite's FDIR (Fault Detection, Isolation, and Recovery) system the node with the corresponding experiment was immediately disabled. This led to high workload for the operators and shorter experimental time. Due to new development there were numerous minor issues. Some of them led to Safe Mode and deactivation of SOLID. However, those issues could be solved through software updates in 2017,

providing more uninterrupted runtime for the experiment in 2018.

The only major downtime of about three months was in time period 08.2019 -10.2019 during preparation of a major software update for the entire satellite bus. The update added a new and powerful system for control and monitoring of all subsystems and payloads, including automatic activation and setup of the SOLID node whenever the satellite is not in Safe Mode. Thus, enables longer operation time for SOLID with less operator interaction.

Table 4 summarizes the number of received reports as well as the identified number of changes on panels 0, 1, 2 and 3 since 2017. As can be seen, there are no changes identified on panel 3. On panels 0 and 1 there are changes identified in 2018 and 2019. Moreover, a large number of changes shows panel 2 in 2017, 2018 and lower number of changes in 2019, 2020.

Table 4: Annual number of reports and identified number of changes (min. / max.) on panels 0, 1, 2 and 3 since 2017

2017	0	1	2	3
Number of data sets	249	306	1371	396
Changes min. /max	0	0	2 / 879	0

2018	0	1	2	3
Number of data sets	1060	1120	3617	1245
Changes min. /max	2	2	2546 / 2804	0

2019	0	1	2	3
Number of data sets	443	446	35	464
Changes min. /max	2	2	12 / 14	0

2020	0	1	2	3
Number of data sets	699	699	5	691
Changes min. /max	0	0	1	0

2021*	0	1	2	3
Number of data sets	235	238	2	234
Changes min. /max	0	0	0	0

*Until 08.07.2021

The changes on panels 0 and 1 in 2018 and 2019 are attributed to abrupt reboots of the SOLID node followed by incorrect initialization of the I2C bus. This led to corrupt status identification of lines on panels 0 and 1. The reason for the reboot events has not been finally clarified. However, such events were also observed on other nodes of the satellite and therefore it is supposed to be a latch-up because of radiation. After subsequent controlled reboots of the SOLID node by the operators and correct initialization of the I2C bus all detection lines were identified intact as before the event. Therefore, it can be concluded, that there were no impacts on panels 0 and 1 in 2018 and 2019.

The changes on panel 2 were identified during the first scan on August 10th 2017 at 07:56:38,1 directly after starting of the SOLID node. All 38 detection lines of one output (output-19, see also Figure 9) were identified as severed lines. However, the next two reports requested by an operator at 08:01:37,6 and 08:01:45,3 on the same day showed intact detection lines. Furthermore, the next report at 08:05:12,6 shows again all lines severed and the next three requests at 09:42:14,5; 09:42:18,2 and 09:42:26,8 again intact detection lines. The state reiterated irregularly in-between intact and severed for the corresponding lines, whereby some data sets show also non-uniform state of the detection lines. This means, that not always all lines were uniformly identified as intact or as severed. The output-19 shows rather a mixed state of the 38 lines. Figure 12 shows an extract of the reports of output-19 in 2017. Here, each cell represents the state of an individual detection line by colour red or white.

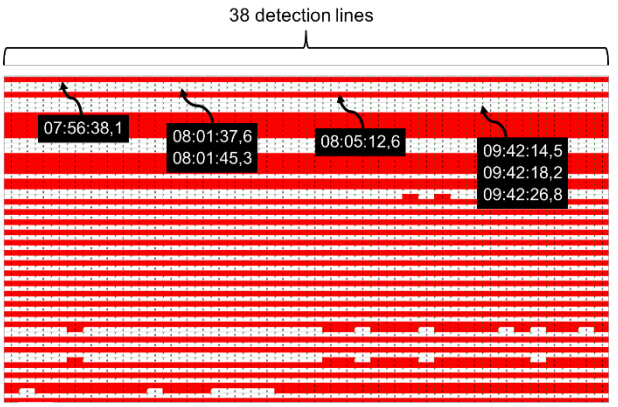

Figure 12: Exemplary extract of SOLID reports for the output-19: white = intact line; red = severed line

In total 1371 reports are available for panel 2 in 2017. For the output-19, the detection lines show a large number of changes with significant fluctuation. Most often all 38 lines are logged as severed. However, some reports show different state of lines (severed lines in the range 0-38) as shown in Figure 12. In summary each individual line of the output-19 changed the state in the range 841-879 in 2017. The reason for that system behaviour is currently under investigation. It is possible, that an impacting object destroyed the feed line of the output-19. Such event could lead to described system

behaviour if a slack joint is generated because of impact for example. However, the probability of such event is negligible low and therefore a hardware related failure like solder joint malfunction on the output expander appears more likely.

Moreover, additional changes of several detection lines were identified on panel 2. Those lines (excluding output-19) changed the state (intact or severed) two to eight times in 2017 in total. Table 5 shows a summary of identified severed detection lines (excluding output-19 for clarity) per scan run on panel 2. All lines before August 11th and after October 6th were identified as intact (not severed). Only the data sets shown within the Table 5 contains severed lines.

Table 5: Identified Number of Severed detection Lines (NSL) on panel 2 per scan in 2017

Date	TM Time	Last change	TM data	NSL
….	….	….	…	0
2017-08-11	07:38:32,5	07:38:31,0	history	0
2017-08-11	07:40:01,6	07:40:00,0	history	1
2017-08-11	07:41:18,7	07:41:17,0	history	0
….	….	….	…	0
2017-09-05	10:36:31,3	10:34:34,0	real time	0
2017-09-05	10:36:36,2	10:34:34,0	real time	242
2017-09-05	10:36:43,7	10:34:34,0	real time	0
2017-09-05	10:36:46,1	10:34:34,0	real time	0
2017-09-05	10:36:48,3	10:34:34,0	real time	0
2017-09-05	10:36:50,7	10:34:34,0	real time	61
2017-09-05	10:36:56,1	10:34:34,0	real time	0
2017-09-05	10:36:58,3	10:34:34,0	real time	0
2017-09-05	10:37:00,7	10:34:34,0	real time	0
2017-09-05	10:37:07,1	10:34:34,0	real time	0
2017-09-05	10:37:12,0	10:34:34,0	real time	161
2017-09-05	10:37:26,7	10:34:34,0	real time	59
2017-09-05	10:37:30,7	10:34:34,0	real time	154
2017-09-05	10:37:36,1	10:34:34,0	real time	0
2017-09-05	10:38:02,6	10:34:34,0	real time	0
2017-09-05	10:38:04,8	10:34:34,0	real time	240
2017-09-05	10:38:10,2	10:34:34,0	real time	0
….	….	….	…	0
2017-09-08	11:19:59,2	11:19:57,0	history	5
2017-09-08	11:20:05,5	11:20:04,0	history	0
….	….	….	…	0
2017-10-06	11:42:41,5	11:42:40,0	history	2
2017-10-06	11:52:09,7	11:52:08,0	history	0
….	….	….	…	0

To lower the amount of data produced, the automatic reports for panel 2 were disabled during the period August 11th 9:50:37, 2 up to September 8th 11:14:29,3. The panel 2 was however scanned continuously and the reports could be requested on demand by operators during ground station contacts. As can be seen from Table 5, the state of the panel was several times requested by an operator via telecommand (real time) on September 5th 2017. Remarkable is however the fact, that the state of lines shows different results even if the reports were requested within some seconds. The state of lines varies in-between 0 and 242 severed lines per scan. At the same time, the timestamp of "Last change" remains constant at 10:34:34,0 and the logged number of changes remains zero (not shown in table). This circumstance is attributed to incorrect system functionality or data transmission on September 5th but not to an impact.

The logged changes on August 11th, September 8th and October 6th are interpreted as readout errors. The subsequently performed automatic scans did not confirm any severed line. The software recognised that as state change consequently. Therefore, new reports were generated based on results of subsequent scans with zero severed lines. Those automatic generated reports are shown as history data in Table 5.

The circumstance shown in Table 5 was finally traced back to telemetry packets received with an experimental ground station setup at Technische Universität Berlin that was operated alongside the primary ground station until October 2017. Due to a software error in the processing of received telemetry, detected transmission errors where not marked correctly as such and were subsequently included in the SOLID data. To exclude the erroneous data in the future the database query collecting SOLID data was updated.

The reports of the following years show further on the same system behaviour regarding the panel 2 where solely output-19 was affected. To reduce the amount of telemetry data the automatically generated reports for panel 2 were disabled permanently. In summary, it can be concluded, that the available reports for panel 2 also don't show an evidence for an impact.

V. EXPECTED NUMBER OF IMPACTS

A set of simulations were run with MASTER-8.0.2 to generate information about expected results regarding the impact probability. Yearly population snapshots were used, starting with the reference population in November 1, 2016 (the latest validated snapshot) through November 1, 2021 for an operational period analysed spanning exactly 4 years from July 2017 to July

2021 (see also chapter IV). For each year, the classical orbital elements of TechnoSat were extracted from TLE, but remained fairly similar throughout the simulation span: in the Sun-synchronous orbit, TechnoSat was on a mean altitude of about 594 km with an inclination of 97.6 degrees.

The resulting Cell-Passage Events (CPE) from MASTER were evaluated to assess the total flux (in units of $1/m^2/\text{year}$), the number of impacts by multiplying the flux with the surface area affected, and the number of penetrating impacts by evaluating of two different Ballistic Limit Equations (BLE):

- Cour-Palais thick glass target (single wall) BLE for a combined thickness of 450 microns (incl. cover glass, solar cell and detection layer), also referred to as "BLE Glass" in the following; and
- McDonnell & Griffiths (single wall) BLE (see also [9]) referred as "Crater SOLID".

Since the satellite is tumbling, three different models were applied to estimate the cross-section of the SOLID surfaces (see Figure 6), to simplify the exact attitude motion of TechnoSat over the simulation span: the *cylinder* model, the *sphere* model and the *surface* model as described in the following.

Cylinder model

The cylinder model would be a justified assumption in a scenario where TechnoSat is stabilised around its yaw axis. As this was not all the time the case, it serves merely for comparison here to the more relevant sphere model (see below). The panels on the different sides experience varying azimuth angles in the horizontal plane and can be approximated by a hollow cylinder, where the outer surface area equals the overall detection area of TechnoSat. The total effective detection area is assumed to be $0.0755\ m^2$. It should also be noted that even though panel 2 was not continuously scanning (see also Table 4), it was fully effective throughout the whole period as the detection of actual impacts, in theory, only requires a single scan at the end of a mission. With more frequent scans, however, a better time resolution is gained, which was the only missing aspect for panel 2. The time dimension is not subject of the analysis in this paper.

For a hollow cylinder with its symmetry axis oriented along the satellite's yaw axis, the cross-section can be computed as:

$$A_c = d \cdot l \cdot \cos h \tag{1}$$

where d is the cylinder's diameter, l is the length and h is the impact elevation with respect to the horizontal plane. The surface area of the combined SOLID detectors is

$$A_{tot} = \pi \cdot d \cdot l = 0.0755\ \text{m}^2, \tag{2}$$

Substituting the product of diameter and length from (2) into (1), the cross-section is computed via:

$$A_c = \frac{A_{tot}}{\pi} \cdot \cos h. \tag{3}$$

For each CPE, the cross-section is computed via Eq. (3) given the impact elevation.

Sphere model

The sphere model is justified under the assumption that there is no stabilised attitude over large periods. In fact, this seems the model coming closest to the behaviour observed for TechnoSat in orbit. It is then assumed that the sensor area is equal to the surface area of a sphere.

Surface model

The surface model is used for comparison, such as the cylinder model, and it is assumed that the individual sides of TechnoSat containing SOLID detectors would face the front (azimuth of 0 deg), left (azimuth of -90 deg), back (azimuth of 180 deg) and right (azimuth of 90 deg) direction, respectively. This would imply the assumption that there was no rotation around the yaw axis and serves to illustrate the directionality effects of space debris impacts.

The results are shown exemplarily for selected impactor diameters in Table 6 for d > 100 µm, Table 7 for d > 150 µm and Table 8 for d > 200 µm. The flux in those tables is given in units of 1/m2/year, whereas the penetrations are computed with the actual applying cross-section for each model used. The minimum particle size to result in a measurable damage size

depends mainly on the impact direction and velocity as outlined before. Cumulating the results for a sphere model over all CPEs results in a penetration likelihood as shown in Figure 13. The BLE Glass refers to the Cour-Palais and the Crater SOLID to the McDonnell & Griffiths Ballistic Limit Equation respectively. The results for the cylinder model are very similar. It can be seen that the objects with a diameter > 100 microns can be expected to be measurable.

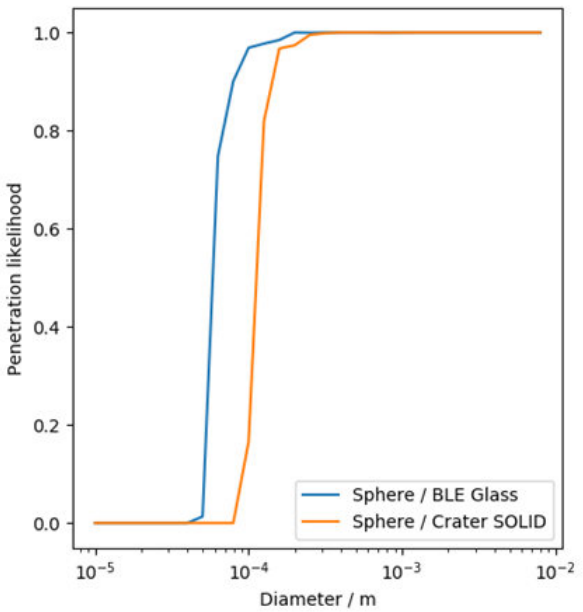

Figure 13: Penetration likelihood for space debris as a function of impactor diameter from MASTER's CPE output at reference epoch

For the reference population, the sphere model in 2016 would lead to an expected number of penetrating impacts (and thus reaching the SOLID detectors) of about 0.45 (>100µm), 0.15 (>150µm) and 0.04 (>200µm) per year for example. For later years, it can be seen how the expected number of impacts increases significantly. This is mainly due to a modelled breakup event in MASTER's future population projection, which in reality never happened. It is therefore reasonable to base interpretations rather on the validated snapshot in 2016 given that no other massive breakup events occurred in the vicinity of TechnoSat in the last few years. Over a period of about 4 years, this would therefore lead to about 2 impacts based on cylinder model as well as on sphere model for objects larger than 100 microns. Note that the sphere model assumes a randomly tumbling satellite, whereas the cylinder model assumes one axis stabilised. As the latter could not be guaranteed over the analysis period, the actual range of results is in between those two models.

It is also necessary to add context on the associated flux uncertainties. MASTER-8 is the first model which provides flux uncertainties that have been derived from the deviations between observed and estimated flux. In MASTER-8, those assessments are made separately for the small and large debris population. While the latter is characterised by ground-based measurements (radar and passive optical instruments), knowledge about the former is based on crater counts on returned surfaces, such as the Hubble Space Telescope's retrieved solar panels. The flux uncertainties are valid at MASTER's reference epoch (November 1, 2016) and are assessed separately for under- and over-predictions of the nominal flux value. For the orbit of TechnoSat in 2016, the 1-σ values are -16% and +192%, respectively. This means that the above nominal value of 2-3 expected impacts for objects larger than 100 µm could be (with 1-σ deviation) 16% lower or even almost double as high. One has to be very careful with these assessments though, as the amount of measurements especially in the size regime above 100 µm is very limited, which in fact was the rationale behind the SOLID development.

VI. CONCLUSION AND OUTLOOK

There is a need for in situ impact detectors with large detection areas which are implemented on as many satellites as possible in different orbits without adding significant cost, mass or complexity to the spacecraft. This would be the only way to create a broad database in the future in order to significantly improve the simulation models and, thus, make the operation of spacecraft safer and cheaper in the long term. A promising step towards achieving this goal is the very first on-orbit test described above with the Solar Panel-based Debris Detector SOLID developed at DLR. The main objective of SOLID is to provide continuously in-situ space debris and meteoroids measurement data from different orbits. The data is required for environmental models (like MASTER (ESA) or ORDEM (NASA)) validation. Furthermore, existing break up models (also used within the environmental models) can be improved, especially regarding the small objects. Validated environmental models will enable engineers to optimize space systems for a given environment e.g. regarding systems shielding or prevention of debris generation. This shall help to reduce the number of objects in space

in the future and to develop step by step a sustainable space environment. To be able to achieve this objective, a high spatial measurement coverage needs to be realized. The required coverage can be achieved by utilization of different spacecraft with SOLID solar panels (mass < 200 g/m²) in different orbits. Satellite constellations like Starlink [32]or OneWeb [33] have the potential to provide significant contribution in environmental data acquisition because of the large number of satellites.

In summary, it can be stated, that the first SOLID on orbit demonstration was quite successful. Since July 2017 the system is still performing in orbit and continues to provide measurement data. However, until July 8th 2021 there was no clear impact observed on the four solar panels. The identified changes on panel 2 are not finally clarified. However, a hardware related failure appears quite likely. The SOLID system showed some weaknesses in the chosen design for the TechnoSat mission. Those are mainly some issues in the hardware - software interaction. For example, a high number of I2C failures as well as the wrong counting of I2C errors were observed. For the cost reasons, COTS components were utilised for the experiment which were not appropriately tested for the space environment. Also, this might be a potential source of partly observed malfunctions. Those issues need to be addressed for the follow-on missions to improve the reliability of the SOLID system.

Table 6: Flux, assessed number of impacts (using the detecting cross-section) and penetration probabilities for objects with object diameter ≥ 100µm

	Impactor sizes > 0.1 mm																					
		2016				2017				2018				2019				2020				2021			
	Flux / 1/m^2/year	Debris	Mets		Total	Debris	Mets		Total	Debris	Mets		Total	Debris	Mets		Total	Debris	Mets		Total	Debris	Mets		Total
		15,25	9,19		24,44	44,53	8,84		53,37	115,91	8,54		124,45	157,25	8,99		166,24	170,75	9,12		179,88	137,73	8,94		146,67
Cylinder model		Debris	Mets		Total	Debris	Mets		Total	Debris	Mets		Total	Debris	Mets		Total	Debris	Mets		Total	Debris	Mets		Total
	No. of impacts / 1/y	0,37	0,16		0,53	1,07	0,16		1,23	2,78	0,15		2,94	3,78	0,16		3,94	4,10	0,16		4,26	3,31	0,16		3,47
	Penetrations (BLE Glass) / 1/y	0,36	0,16		0,52	1,05	0,15		1,20	2,72	0,15		2,87	3,65	0,15		3,81	3,96	0,16		4,12	3,19	0,15		3,35
	Penetrations (Crater SOLID) / 1/y	0,34	0,13		0,46	0,92	0,12		1,04	2,42	0,12		2,53	3,19	0,12		3,31	3,54	0,13		3,66	2,95	0,12		3,07
	Prob. of no impact		58,9%				29,3%				5,3%				2,0%				1,4%				3,1%		
	Prob. of no penetration (BLE Glass)		59,7%				30,2%				5,7%				2,2%				1,6%				3,5%		
	Prob. of no penetration (Crater SOLID)		62,9%				35,3%				7,9%				3,6%				2,6%				4,6%		
Sphere model		Debris	Mets		Total	Debris	Mets		Total	Debris	Mets		Total	Debris	Mets		Total	Debris	Mets		Total	Debris	Mets		Total
	No. of impacts / 1/y	0,29	0,17		0,46	0,84	0,17		1,01	2,19	0,16		2,35	2,97	0,17		3,14	3,22	0,17		3,40	2,60	0,17		2,77
	Penetrations (BLE Glass) / 1/y	0,28	0,17		0,45	0,82	0,17		0,99	2,14	0,16		2,30	2,87	0,17		3,04	3,11	0,17		3,28	2,51	0,17		2,68
	Penetrations (Crater SOLID) / 1/y	0,27	0,15		0,42	0,72	0,15		0,87	1,90	0,14		2,04	2,51	0,15		2,66	2,78	0,15		2,93	2,32	0,15		2,47
	Prob. of no impact		63,1%				36,5%				9,5%				4,3%				3,4%				6,3%		
	Prob. of no penetration (BLE Glass)		63,5%				37,3%				10,1%				4,8%				3,8%				6,9%		
	Prob. of no penetration (Crater SOLID)		65,7%				41,8%				13,0%				7,0%				5,3%				8,5%		
Surface model		Front	Left	Rright	Back	Front	Left	Rright	Back	Front	Left	Rright	Back	Front	Left	Rright	Back	Front	Left	Rright	Back	Front	Left	Rright	Back
	No. of impacts / 1/y	0,32	0,11	0,10	0,01	0,75	0,25	0,24	0,01	1,88	0,52	0,50	0,01	2,51	0,71	0,67	0,01	2,73	0,73	0,75	0,01	2,23	0,59	0,57	0,01
	Penetrations (BLE Glass) / 1/y	0,30	0,09	0,09	0,01	0,70	0,22	0,20	0,01	1,78	0,42	0,41	0,01	2,36	0,54	0,53	0,01	2,59	0,59	0,60	0,01	2,13	0,48	0,45	0,01
	Penetrations (Crater SOLID) / 1/y	0,25	0,05	0,05	0,00	0,58	0,09	0,10	0,00	1,53	0,20	0,19	0,00	2,03	0,22	0,22	0,00	2,20	0,25	0,24	0,00	1,88	0,24	0,24	0,00
	Prob. of no impact		58,4%				28,7%				5,5%				2,0%				1,5%				3,4%		
	Prob. of no penetration (BLE Glass)		61,2%				32,3%				7,3%				3,2%				2,3%				4,6%		
	Prob. of no penetration (Crater SOLID)		70,6%				46,0%				14,5%				8,4%				6,7%				9,4%		

Table 7: Flux, assessed number of impacts (using the detecting cross-section) and penetration probabilities for objects with object diameter ≥ 150µm

	Impactor sizes > 0.15 mm																					
		2016				2017				2018				2019				2020				2021			
	Flux / 1/m^2/year	Debris	Mets		Total	Debris	Mets		Total	Debris	Mets		Total	Debris	Mets		Total	Debris	Mets		Total	Debris	Mets		Total
		4,38	2,40		6,78	12,74	2,31		15,05	32,93	2,24		35,17	35,21	2,37		37,59	42,16	2,39		44,55	45,25	2,34		47,59
Cylinder model		Debris	Mets		Total	Debris	Mets		Total	Debris	Mets		Total	Debris	Mets		Total	Debris	Mets		Total	Debris	Mets		Total
	No. of impacts / 1/y	0,12	0,05		0,16	0,33	0,04		0,38	0,86	0,04		0,90	0,92	0,05		0,96	1,10	0,05		1,14	1,18	0,05		1,22
	Penetrations (BLE Glass) / 1/y	0,11	0,05		0,16	0,33	0,04		0,37	0,85	0,04		0,89	0,91	0,05		0,95	1,09	0,05		1,13	1,16	0,05		1,21
	Penetrations (Crater SOLID) / 1/y	0,11	0,05		0,16	0,32	0,04		0,37	0,84	0,04		0,88	0,88	0,05		0,93	1,08	0,05		1,12	1,14	0,04		1,18
	Prob. of no impact		84,9%				68,7%				40,6%				38,2%				31,8%				29,4%		
	Prob. of no penetration (BLE Glass)		85,1%				68,8%				41,0%				38,6%				32,1%				29,9%		
	Prob. of no penetration (Crater SOLID)		85,2%				69,2%				41,6%				39,6%				32,5%				30,7%		
Sphere model		Debris	Mets		Total	Debris	Mets		Total	Debris	Mets		Total	Debris	Mets		Total	Debris	Mets		Total	Debris	Mets		Total
	No. of impacts / 1/y	0,09	0,05		0,15	0,26	0,05		0,33	0,67	0,05		0,78	0,72	0,05		0,84	0,86	0,05		0,99	0,93	0,05		1,06
	Penetrations (BLE Glass) / 1/y	0,09	0,05		0,15	0,26	0,05		0,33	0,67	0,05		0,77	0,71	0,05		0,82	0,86	0,05		0,98	0,91	0,05		1,04
	Penetrations (Crater SOLID) / 1/y	0,09	0,05		0,15	0,26	0,05		0,33	0,66	0,05		0,76	0,69	0,05		0,80	0,85	0,05		0,97	0,89	0,05		1,02
	Prob. of no impact		86,1%				71,6%				45,8%				43,4%				37,2%				34,7%		
	Prob. of no penetration (BLE Glass)		86,1%				71,7%				46,2%				43,9%				37,5%				35,3%		
	Prob. of no penetration (Crater SOLID)		86,2%				72,0%				46,7%				44,8%				37,8%				36,1%		
Surface model		Front	Left	Rright	Back	Front	Left	Rright	Back	Front	Left	Rright	Back	Front	Left	Rright	Back	Front	Left	Rright	Back	Front	Left	Rright	Back
	No. of impacts / 1/y	0,10	0,03	0,04	0,00	0,23	0,07	0,07	0,00	0,58	0,18	0,14	0,00	0,61	0,16	0,19	0,00	0,76	0,17	0,18	0,00	0,79	0,19	0,20	0,00
	Penetrations (BLE Glass) / 1/y	0,09	0,02	0,04	0,00	0,23	0,07	0,07	0,00	0,57	0,16	0,13	0,00	0,59	0,15	0,18	0,00	0,75	0,16	0,16	0,00	0,78	0,17	0,18	0,00
	Penetrations (Crater SOLID) / 1/y	0,09	0,02	0,04	0,00	0,22	0,06	0,06	0,00	0,55	0,14	0,12	0,00	0,57	0,13	0,16	0,00	0,74	0,14	0,14	0,00	0,76	0,15	0,17	0,00
	Prob. of no impact		85,0%				68,6%				40,7%				38,4%				32,9%				30,6%		
	Prob. of no penetration (BLE Glass)		85,3%				69,6%				42,2%				39,8%				34,2%				32,2%		
	Prob. of no penetration (Crater SOLID)		86,1%				71,2%				44,4%				42,3%				35,8%				34,1%		

Table 8: Flux, assessed number of impacts (using the detecting cross-section) and penetration probabilities for objects with object diameter ≥ 200µm

	Impactor sizes > 0.2 mm																							
		2016				2017				2018				2019				2020				2021			
	Flux / 1/m^2/year	Debris	Mets	Total		Debris	Mets	Total		Debris	Mets	Total		Debris	Mets	Total		Debris	Mets	Total		Debris	Mets	Total	
		0,89	0,81	1,70		1,68	0,78	2,46		5,39	0,76	6,15		9,12	0,79	9,91		10,32	0,80	11,13		9,92	0,79	10,71	
Cylinder model		Debris	Mets	Total		Debris	Mets	Total		Debris	Mets	Total		Debris	Mets	Total		Debris	Mets	Total		Debris	Mets	Total	
	No. of impacts / 1/y	0,02	0,02	0,04		0,04	0,01	0,06		0,14	0,01	0,15		0,24	0,02	0,25		0,27	0,02	0,28		0,26	0,02	0,27	
	Penetrations (BLE Glass) / 1/y	0,02	0,02	0,04		0,04	0,01	0,06		0,14	0,01	0,15		0,24	0,02	0,25		0,27	0,02	0,28		0,26	0,02	0,27	
	Penetrations (Crater SOLID) / 1/y	0,02	0,02	0,04		0,04	0,01	0,06		0,14	0,01	0,15		0,23	0,02	0,25		0,26	0,02	0,28		0,25	0,02	0,27	
	Prob. of no impact		96,2%				94,3%				85,7%				77,6%				75,2%				76,0%		
	Prob. of no penetration (BLE Glass)		96,2%				94,4%				85,7%				77,8%				75,4%				76,2%		
	Prob. of no penetration (Crater SOLID)		96,2%				94,4%				85,9%				78,0%				75,6%				76,3%		
Sphere model		Debris	Mets	Total		Debris	Mets	Total		Debris	Mets	Total		Debris	Mets	Total		Debris	Mets	Total		Debris	Mets	Total	
	No. of impacts / 1/y	0,02	0,02	0,04		0,03	0,02	0,05		0,11	0,02	0,13		0,19	0,02	0,20		0,21	0,02	0,23		0,20	0,02	0,22	
	Penetrations (BLE Glass) / 1/y	0,02	0,02	0,04		0,03	0,02	0,05		0,11	0,02	0,12		0,18	0,02	0,20		0,21	0,02	0,23		0,20	0,02	0,22	
	Penetrations (Crater SOLID) / 1/y	0,02	0,02	0,04		0,03	0,02	0,05		0,11	0,02	0,12		0,18	0,02	0,20		0,21	0,02	0,22		0,20	0,02	0,22	
	Prob. of no impact		96,6%				95,1%				88,1%				81,6%				79,6%				80,3%		
	Prob. of no penetration (BLE Glass)		96,6%				95,1%				88,3%				81,8%				79,8%				80,4%		
	Prob. of no penetration (Crater SOLID)		96,6%				95,1%				88,4%				81,9%				79,9%				80,5%		
Surface model		Front	Left	Rright	Back	Front	Left	Rright	Back	Front	Left	Rright	Back	Front	Left	Rright	Back	Front	Left	Rright	Back	Front	Left	Rright	Back
	No. of impacts / 1/y	0,02	0,01	0,01	0,00	0,04	0,01	0,01	0,00	0,10	0,02	0,02	0,00	0,17	0,04	0,04	0,00	0,19	0,04	0,04	0,00	0,18	0,04	0,05	0,00
	Penetrations (BLE Glass) / 1/y	0,02	0,01	0,01	0,00	0,04	0,01	0,01	0,00	0,10	0,02	0,02	0,00	0,16	0,04	0,04	0,00	0,19	0,04	0,04	0,00	0,18	0,04	0,04	0,00
	Penetrations (Crater SOLID) / 1/y	0,02	0,01	0,01	0,00	0,04	0,01	0,01	0,00	0,10	0,02	0,02	0,00	0,16	0,04	0,04	0,00	0,18	0,04	0,04	0,00	0,17	0,04	0,04	0,00
	Prob. of no impact		96,3%				94,5%				86,2%				78,2%				75,8%				76,7%		
	Prob. of no penetration (BLE Glass)		96,3%				94,5%				86,5%				78,5%				76,2%				77,1%		
	Prob. of no penetration (Crater SOLID)		96,4%				94,6%				86,8%				79,0%				76,7%				77,6%		

VII. REFERENCES

[1] V. Braun, A. Horstmann, S. Lemmens, C. Wiedemann, and L. Böttcher, "Recent developments in space debris environment modelling, verification and validation with MASTER," in *8th European Conference on Space Debris*, 20 - 23 April Darmstadt, Germany, 2021.

[2] A. Horstmann, S. Hesselbach, and C. Wiedemann, "Final Report: Enhancement of S/C Fragmentation and Environment Evolution Models," Institute of Space Systems (IRAS) DD-0045, 26th Aug. 2020. [Online]. Available: https://sdup.esoc.esa.int/master/downloads

[3] J. Kuitunen *et al.,* "DEBIE - first standard in-situ debris monitoring instrument," in *Proceedings of the Third European Conference on Space Debris*, Darmstadt, Germany, 2001.

[4] G. Drolshagen, "Initial Results from the DEBIE-1 Impact Detector Onboard PROBA: ESA/TOS-EMA March 2003," 2003.

[5] J. P. Schwanethal, N. McBride, S. F. Green, McDonnell, J. A. M., and G. Drolshagen, "ANALYSIS OF IMPACT DATA FROM THE DEBIE (DEBRIS IN-ORBIT EVALUATOR) SENSOR IN POLAR LOW EARTH ORBIT," in *Proc. of the 4th European Conference on Space Debris, 18-20 April, 2005, ESA/ESOC, Darmstadt, Germany*, Darmstadt, Germany, 2005.

[6] G. Drolshagen, "Hypervelocity impact effects on spacecraft," in *Proceedings of the Meteoroids 2001 Conference: 6-10 August 2001, Swedish Institute of Space Physics, Kiruna, Sweden*, 2001, p. 533 - 541. Accessed: Dec. 28 2013. [Online]. Available: http://adsabs.harvard.edu/full/2001ESASP.495.533D

[7] S. Flegel, J. Gelhaus, M. Möckel, and Wiedemann, C, Kempf, D., "Maintenance of the ESA MASTER Model," Final Report, Institute of Aerospace Systems (ILR), Technische Universität Braunschweig (TUBS), May. 2011.

[8] S. Stabroth, M. Oswald, C. Wiedemann, H. Klinkrad, and P. Vörsmann, "Explanation of the "May Swarm" signature in the LDEF IDE impact data," *Aerospace Science and Technology*, vol. 11, 2-3, pp. 253–257, 2007, doi: 10.1016/j.ast.2007.02.003.

[9] W. Bauer, "Space-Debris-Detektion zur Validierung von Simulations-Modellen: Forschungsbericht 2015-08," Dissertation, Technische Universität Braunschweig, 2015.

[10] J. McDonnell *et al.,* "Meteoroid and debris flux and ejecta models, Final Report, ESA Contract No. 11887/96/NL/JG," ESA, 1998.

[11] J. McDonnell, "Post-Flight Impact Analysis of HST Solar Arrays - 2002 Retrieval, Final Report, ESA Contract No. 16283/NL/LvH," ESA, 2005.

[12] G. Drolshagen, "Effects of hypervelocity impacts from meteoroids and space debris,," ESA TEC-EES/2005.302/GD, Jun. 2005.

[13] S. Flegel, K. Letsch, and H. Krag, "Theoretical analysis of south-staring Beampark configurations for the TIRA system," *CEAS Space J*, vol. 7, no. 3, pp. 375–387, 2015, doi: 10.1007/s12567-015-0085-1.

[14] J.-C. Liou, M. J. Matney, Anz-Meador, P. D., D. Kessler, M. Jansen, and J. R. Theall, "The New NASA Orbital Debris Engineering Model ORDEM2000," NASA/TP—2002-210780, May. 2002.

[15] M. Matney and et al., "The NASA orbital debris engineering model 3.1: development, verification, and validation." 1st International Orbital Debris Conference, Sugar Land," in *1st International Orbital Debris Conference*, Sugar Land, TX. 2019.

[16] W. Bauer and O. Romberg, "Solargenerator," DE-Patent DE102012000260.

[17] W. Bauer and O. Romberg, "Solar Generator," US Patent 8593165B2.

[18] W. Bauer, O. Romberg, A. Pissarskoi, C. Wiedemann, and P. Vörsmann, "In orbit debris-detection based on solar panels," *CEAS Space J*, vol. 5, 1-2, pp. 49–56, 2013, doi: 10.1007/s12567-013-0039-4.

[19] W. Bauer, O. Romberg, C. Wiedemann, G. Drolshagen, and P. Vörsmann, "Development of in-situ Space Debris Detector," *Advances in Space Research*, vol. 54, no. 9, pp. 1858–1869, 2014, doi: 10.1016/j.asr.2014.07.035.

[20] W. Bauer, "SOLID-A solar panel based impact detector," Mar. 2 2021. [Online]. Available: https://indico.esa.int/event/370/

[21] W. Bauer, O. Romberg, and R. Putzar, "Experimental verification of an innovative debris detector," *Acta Astronautica*, vol. 117, pp. 49–54, 2015, doi: 10.1016/j.actaastro.2015.07.008.

[22] M. F. Barschke, K. Gordon, M. Lehmann, and K. Brieß, "'The TechnoSat mission for on-orbit technology demonstration', .," in *in Proceedings of the 65th German Aerospace Congress*, Braunschweig, Germany, 2016.

[23] M. F. Barschke *et al.,* "Initial orbit results from the TUBiX20 platform," *Acta Astronautica*, vol. 167, pp. 108–116, 2020, doi: 10.1016/j.actaastro.2019.10.034.

[24] M. F. Barschke *et al.,* "TechnoSat - Results from the first 18 months of operation," in *Proceedings of the 12th IAA Symposium on Small Satellites for Earth Observation*, 2019.

[25] M. Barschke *et al.,* "Initial results from the TechnoSat in-orbit demonstration mission," in *Proceedings of the 32nd AIAA/USU Conference on Small Satellites, Logan, USA, 2018.*, 2018.
[26] Technischen Universität Berlin, *TechnoSat.* [Online]. Available: https://www.tu-berlin.de/?133828
[27] Spaceflight Now, *Soyuz rolled out for launch of multinational satellite cluster.* [Online]. Available: https://spaceflightnow.com/2017/07/12/soyuz-rolled-out-for-launch-of-multinational-satellite-cluster/
[28] Deutsches Zentzum für Luft- und Raumfahrt (DLR), *Ein-bau von Tech-no-Sat in die Ra-ke-te.* [Online]. Available: https://www.dlr.de/content/de/artikel/news/2017/20170714_die-kleinsatelliten-technosat-und-flying-laptop-starten-erfolgreich-in-den-weltraum_23218.html
[29] K. Gordon, M. F. Barschke, and P. Werner, Eds., *Upgrading TUBiX20 – bringing TechnoSat flight experience into the TUBIN mission,: Proceedings of the Small Satellites Systems and Services Symposium*, 2018.
[30] W. Bauer *et al.,* "DEBRIS IN-SITU IMPACT DETECTION BY UTILIZATION OF CUBE-SAT SOLAR PANELS," in *The 4S SYMPOSIUM*, Valletta, Malta, May. 2016.
[31] University of Wuerzburg, *Rodos (operating system).* [Online]. Available: https://en.wikipedia.org/wiki/Rodos_(operating_system)
[32] Starlink © 2021, *WORLD'S MOST ADVANCED BROADBAND INTERNET SYSTEM.* [Online]. Available: https://www.starlink.com/satellites
[33] oneweb.net, *Connected As One.* [Online]. Available: https://oneweb.net/